Composites Science and Technology 232 (2023) 109873

Contents lists available at ScienceDirect

Composites Science and Technology

journal homepage: www.elsevier.com/locate/compscitech

Numerical analysis of fracture in interpenetrating phase composites based on crack phase field model

Wei Fan [a], Hua Yang [b,c,**], Ambrose C. Taylor [a,*]

[a] Department of Mechanical Engineering, Imperial College London, South Kensington Campus, London, SW7 2AZ, UK
[b] Institute of Mechanics, Technische Universität Berlin, Einsteinufer 5, Berlin, 10587, Germany
[c] School of Mechanical Engineering, Hebei University of Technology, Tianjin, 300401, PR China

ARTICLE INFO

Keywords:
Polymer-matrix composites (PMCs)
Fracture toughness
Mechanical properties
Damage tolerance
Material modelling

ABSTRACT

A numerical model based on crack phase field analysis is introduced to study the quasi-static fracture process in interpenetrating phase composites (IPCs). Materials were considered elastic solids, and the interface was assumed to be perfectly bonded. Tougher and stiffer tougheners lead to more fracture in the brittle phase, but less fracture in the toughening phase. Thus, the overall fracture performance results from competition between increasing breakage in the brittle phase and declining breakage in the toughening phase. The toughening mechanisms are discussed from both stress-strain and crack topology viewpoints. The toughening phase transfers the load from the crack tip to the whole domain until the maximum stress is reached, and impeded crack growth occurs afterwards. The load transferring and impediment effects made the brittle phase engage in fracture, and several crack propagation patterns were identified for the sacrificial fracture behaviour, namely, crack deflection, crack bridging, crack branching, microcracking and crack blocking. Moreover, fracture in three different microstructures (co-continuous, particle-reinforced, laminar) was compared, and the most effective toughening morphology depends on the tougheners and the loading states. This methodology enables optimum microstructures to be identified to achieve high toughness in aerospace and energy generation applications, increasing safety and reducing weight.

1. Introduction

Preparing composites is an important strategy to enhance the mechanical performance of brittle materials with desired functionality. According to the morphology of the brittle matrix and tougheners, composites are divided into three types: Interpenetrating Phase Composites (IPCs), Particle-Reinforced Composites (PRCs), and Laminar Composites (LCs). IPCs are composed of two phases with a 3D spatially interconnected structure, and each phase is self-supporting. Benefitting from the co-continuous structures, IPCs enable an exciting design strategy which has been demonstrated in structural materials [1–3], solid batteries [4], semiconductors industry [5,6], biomedical materials [7], and soft actuators [8–10].

In applications such as aerospace structures, the mechanical properties of IPCs are of great significance, and have been extensively researched. Experiments using different composite systems have demonstrated that, in comparison with a particle-reinforced morphology, the co-continuous morphology greatly enhanced fracture toughness [11–14], impact strength [11,12,15–17], and fatigue properties [18]. Simulation models have also been proposed to predict the mechanical behaviours of IPCs. Based on the element free Galerkin method, Agarwal et al. [19] used the Ramberg-Osgood model to simulate the elastoplastic behaviour, and a progressive damage model to mimic the failure of IPCs. Xie et al. [20] used a 3D finite element (FE) model to generate IPCs and investigated the elastic and elastoplastic behaviours. Zhang and colleagues [21] numerically predicted the stress-strain curves and von Mises stress maps of various 3D-printed IPCs under compression.

The toughening mechanisms of IPCs have also been investigated. Cavitation and void growth [13,22], as well as plastic deformation [13,17,23], were demonstrated, and the effect of interface on them was studied in PLA/PA11 [17] and PLA/PMMA grafted natural rubber thermoplastic vulcanizates [13]. When the interface was weak, the crack nucleates and grows along the interface zone, leading to a brittle

** Corresponding author. Institute of Mechanics, Technische Universität Berlin, Einsteinufer 5, Berlin, 10587, Germany.
* Corresponding author.
E-mail addresses: hua.yang@hebut.edu.cn (H. Yang), a.c.taylor@imperial.ac.uk (A.C. Taylor).

https://doi.org/10.1016/j.compscitech.2022.109873
Received 19 October 2022; Accepted 8 December 2022
Available online 10 December 2022

fracture surface from the pull-out effect. When the interfacial adhesion was improved, the fracture surface became much rougher because of the formation of highly stretched bridging microfibrils. In addition, based on the crack growth topology, crack deflection, crack bridging and microcracking [14,22,24] were also reported.

Although the above studies provide good explanations for the superior mechanical properties of IPCs, they have not placed any emphasis on the role of the co-continuous microstructures. Recently, sacrificial fracture behaviours have been proposed in interconnected structures [8, 25–27]. The sacrificing concept has been previously reported in double-network (DN) hydrogels and elastomers [28–31], which are composed of two interconnected polymeric networks with distinct mechanics, and display much higher fracture energy compared with traditional gels. Sacrificial behaviour occurs when the stiff network breaks massively, acting as sacrificial bonds, while the soft network maintains the structural integrity upon stretching. The load between the two networks is transferred via molecular interactions such as physical crosslinking. Considering that IPCs have a similar double-phase network, it is not hard to imagine that sacrificial toughening mechanisms exist in co-continuous composites.

In this work, we explore the mechanical behaviours and sacrificial toughening mechanisms in IPCs via simulations. A crack phase field model is employed to study tensile fracture in epoxy IPCs formed by spinodal decomposition. This paper presents a description of the numerical models applied to investigate the toughening mechanisms and quantitative evaluations of fractures in co-continuous structures. Moreover, fracture in different microstructures was compared to identify the most effective morphology. This methodology enables industry and researchers to identify the optimum microstructures for high toughness in aerospace and energy generation applications, increasing safety and reducing weight.

2. Methods

2.1. Simulation setup

Considering the complexity of co-continuous structures, it is hard to sketch the morphology manually. In this study, a two-step simulation strategy was adopted. The morphology of brittle matrix and tougheners were obtained by simulation of the phase separation process and then used as the basis for the fracture analysis. A domain size of 100 μm * 100 μm was selected as being suitable to capture the features of the typical microstructure and was meshed into identical square elements with element size h_{FEM}, as shown in Fig. 1a. A value of $h_{FEM} = 1$ μm was used for the numerical simulation, and $h_{FEM} = 5$ μm is shown in Fig. 1a for clear viewing.

First, algorithms to generate the morphology were implemented, and accordingly, the domain was divided into an epoxy-rich phase (EP) and a toughening phase (TP) with the same volume fraction. The interface between phases was considered perfect bonding. Fig. 1b displays the microstructures investigated in this study: co-continuous microstructure (IPC), particulate microstructure (PRC) and laminar microstructure (LCV or LCH). For co-continuous and particulate microstructures, five IPC specimens and five PRC specimens were randomly generated. The simulation details are given in Section 2.2, and the obtained morphologies are shown in Fig. S1 in the supporting information. For the laminar microstructure, laminar composite (LC) specimens were generated via customized codes. When the crack direction was perpendicular to the laminar alignments (vertical), the specimen is denoted LCV, and when parallel (horizontal) is denoted LCH. It should be noted that LCV specimen and LCH specimen are unique, so only a single microstructure is required for analysis.

In the fracture simulation, a 20-μm-long single-edge notch was introduced, and the crack tip was always located in the epoxy-rich phase. The specimens were fixed at the bottom boundary and stretched at the top boundary with a constant increment size of 1×10^{-6} mm (Fig. 1c). For a piece of single-phase material, the stress-strain curve and crack pattern are presented in Fig. 1d, and the toughness Γ is defined as the area under the stress-strain curve. The details of the crack phase field method are given in Section 2.3.

2.2. Simulating morphology development via phase separation

In a binary system, an initially uniform blend can divide into multiple phases upon heating or reaction. A mathematical description of the morphology evolution is given by the Cahn-Hilliard equation [32],

$$\frac{\partial c}{\partial t} = M\Delta\left[\frac{df(c)}{dc} - \gamma\Delta c\right] \tag{1}$$

where c is the concentration of one component, t is time, M is the mobility coefficient, γ is a constant related to interphase thickness, and $f(c)$ is a free energy density function. In the phase separation simulation, periodic boundary conditions were adopted for the domain. A time step $dt = 5 \times 10^{-6}$ s, mobility coefficient $M = 1$ m^2/s, $\gamma = 0.01$ m^2/s, and $f(c) = 100 \cdot c^2 \cdot (1-c)^2$ were used. An initial c value was randomly assigned, with normal distribution $N(c_0, 0.01)$, to each

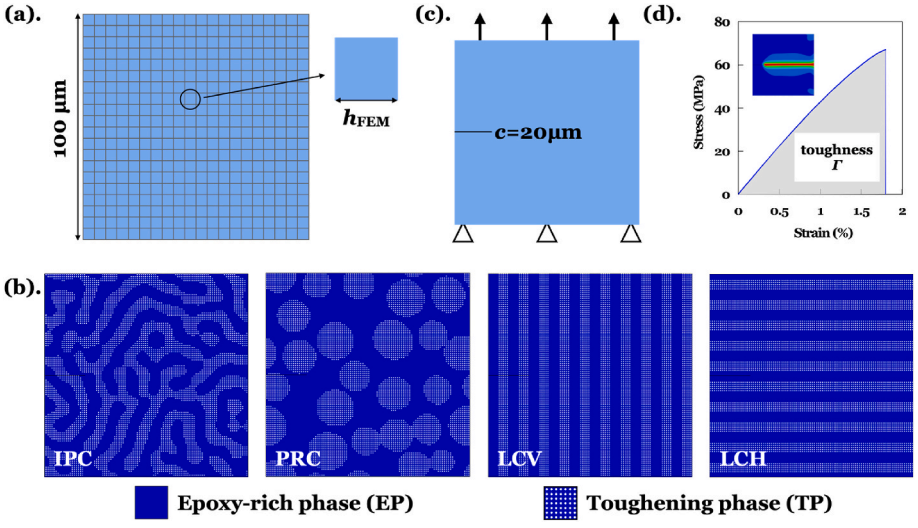

Fig. 1. Schematic of fracture simulation. (a) The domain is meshed by identical square elements. $h_{FEM} = 5$ μm for clear viewing; (b) Microstructures investigated in this study; (c) Boundary conditions for fracture analysis; (d) Simulation results from a single-phase material.

element at $t = 0$. Depending on the initial concentration c_0, the resulting phase morphology can be either particulate (Fig. 2a) or co-continuous (Fig. 2b). The numerical simulation of phase separation was performed using an open-source Python code provided by FEniCS [33,34]. A cut-off value of concentration was applied to distinguish the epoxy-rich phase and toughening phase, and the cut-off value was adjusted to ensure that the two phases have the same volume fraction.

2.3. Crack phase field analysis

An open-source Abaqus implementation of the crack phase field analysis [35] was employed to investigate the fracture of the composites. In the model, a crack was denoted by a continuous scalar $d \in [0, 1]$, where $d = 0$ represents intact material and $d = 1$ represents the fully broken state, and its characteristic width was considered as constant, $l_c = 2h_{FEM} = 2$ μm. Materials were taken as elastic solids, and their mechanical behaviours were defined by two parameters, tensile modulus E and fracture surface energy density g_c. To investigate the effect of toughening, we kept $g_{c,\,EP} = 40$ J/m^2 and $E_{EP} = 4$ GPa, and changed $g_{c,\,TP}$ and E_{TP}. As shown in Table S1, the tougheners with different $g_{c,TP}$ and E_{TP} were denoted as TPij, i = A, B, C, D standing for $g_{c,TP} = 500$, 200, 80, 40 J/m^2, and $j = 1$, 2, 3, 4 standing for $E_{TP} = 4$, 2, 1, 0.5 GPa. For example, TPA1 means tougheners with $g_{c,TP} = 500$ J/m^2 and $E_{TP} = 4$ GPa. The IPC-TPD1 specimens were identical to the EP specimen. The effects of the model parameters on the stress-strain behaviours of the tougheners are presented in Fig. S2.

3. Results and discussion

3.1. Relationship between stress-strain curves and co-continuous structures

The tensile behaviour of the EP and the IPC-TPA2 specimens are presented in Table 1 and Fig. 3. Compared with the EP specimen, the IPC specimens are much stronger and tougher, but less stiff. This is as expected, in accordance with the properties of the tougheners. Crack patterns are presented at four selected points for each IPC specimen: crack nucleation, maximum stress, catastrophic crack propagation, and final rupture. Crack nucleation (point 1) is defined when the maximum crack phase field d is larger than 0.9 within the whole domain. Although the crack nucleated in the epoxy-rich phase (Fig. 3, a1-e1), the IPCs show a larger strain at crack nucleation and greater Ultimate Tensile Strength (*UTS*) compared with the EP specimen. These are because the load is transferred from the crack tip to the whole specimen via the continuous TP networks (Fig. 3 a2-e2), and the load transferring effect is less likely to be affected by the co-continuous patterns. Afterwards, unstable crack growth in EP network leads to a dramatically reduced stress (point 3), and upon further stretching, the final rupture of the specimen occurs (point 4). At this stage, the TP network was not able to relieve the stress concentration effectively and played the role of the impediment to crack growth. In the IPC1 and IPC2 specimens, a slight toughening effect after point 2 can be observed, because crack growth was hindered by the tougheners (Fig. 3, a3 & b3). After the crack penetrated the impeded tougheners, the final rupture occurred quickly (Fig. 3, a4 & b4). Compared with the other IPC-TPA2 specimens, they have similar toughness values due to the similar crack growth processes. The IPC3 specimen showed the lowest toughness since the crack was barely impeded after the *UTS*, (Fig. 3, c1-c4). The difference between the strain at point 2 and the strain at point 4 is only 0.3%, indicating a large portion of brittle fracture with little toughening effect. In the IPC4 specimen, the maximum tensile strength and strain at crack nucleation were observed, as the precut crack was blocked by the tougheners. In the IPC5 specimen, the crack propagated in the parallel aligned EP networks and formed extensive crack branches (Fig. 3, e2 & e3). This special co-continuous pattern made IPC5 specimen the toughest specimen among this group, being almost twice as tough as the IPC3 specimen. Above all, the crack resistance after point 2 and the strain at rupture are dominated

Table 1
Mechanical properties of IPC specimens with TPA2 tougheners.

#	E (GPa)[a]	*UTS* (MPa)	ε_{rup} (%)	Γ (MJ/m^3)
EP	4.50	65.41	2.04	0.74
IPC1	3.15	93.40	4.72	2.67
IPC2	3.13	93.70	5.16	2.51
IPC3	3.14	92.90	3.98	2.09
IPC4	3.16	103.04	6.72	3.07
IPC5	3.15	97.78	9.78	3.89

[a] Modulus is calculated as the slope between points at $\varepsilon = 0$ & $\varepsilon = 0.1\%$.

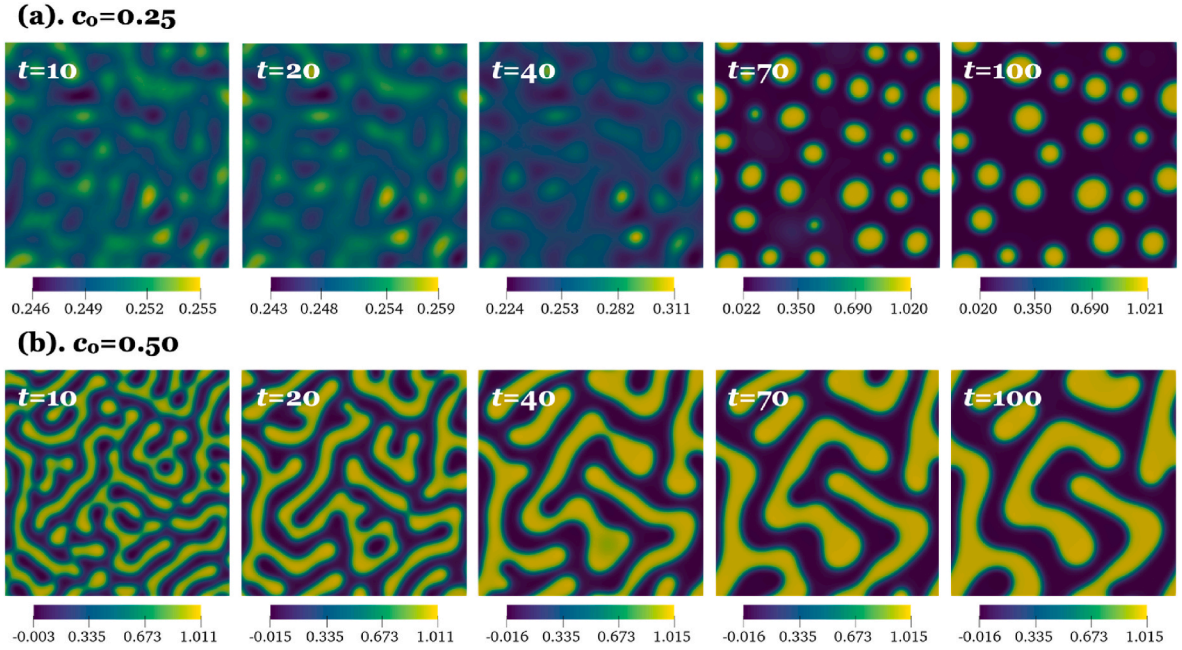

Fig. 2. Morphology development of (a) particulate microstructure, and (b) co-continuous microstructure via phase separation depending on the initial concentration, c_0.

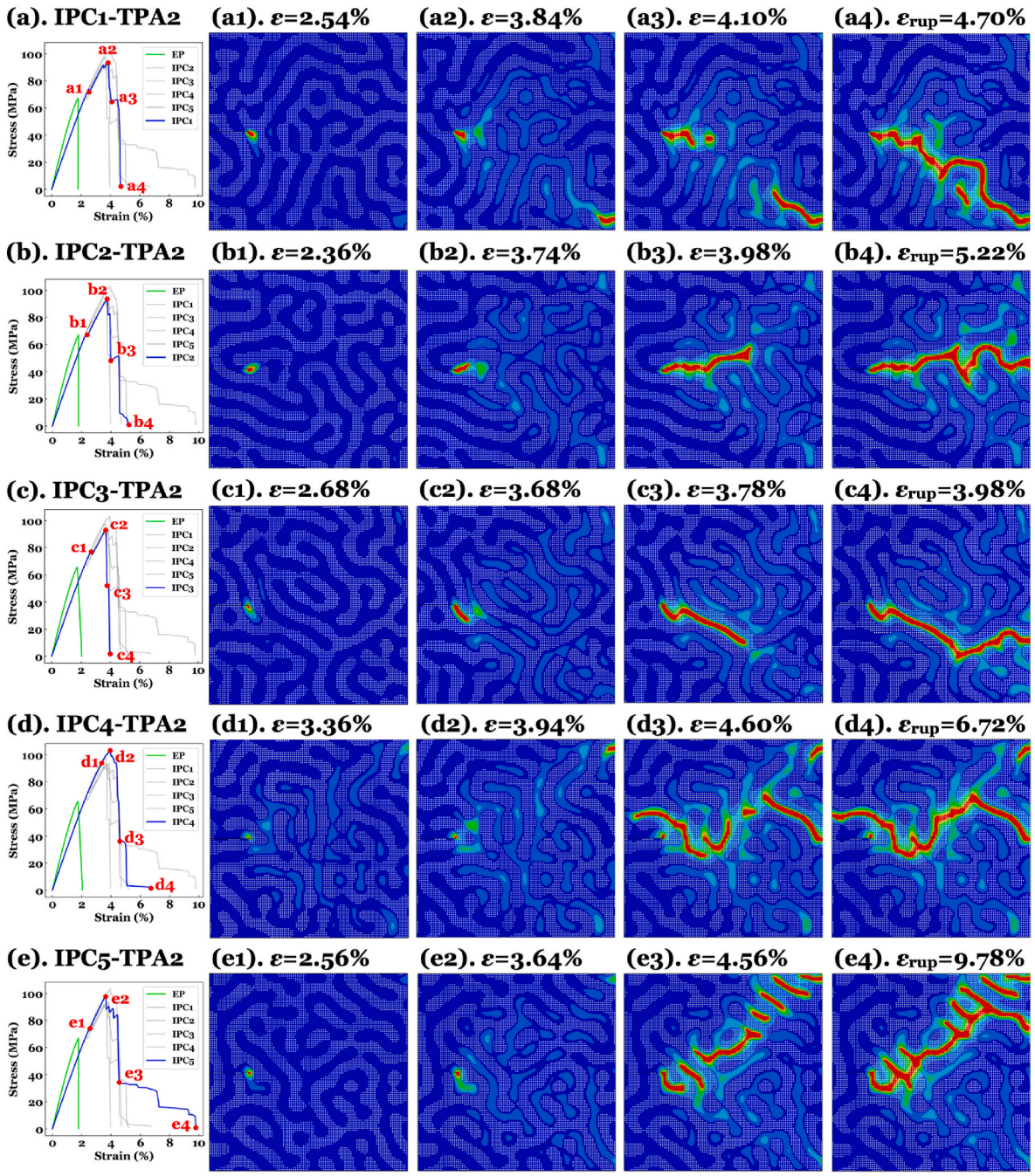

Fig. 3. The relationship between co-continuous patterns and stress-strain curves in the TPA2 group. (a) IPC1; (b) IPC2; (b) IPC3; (d) IPC4; (e) IPC5.

by the impediment effect of the tougheners, which is largely affected by the microstructure of the co-continuous patterns.

3.2. Mechanical performance in IPCs with different tougheners

Fig. 4 presents the mechanical properties of the IPC specimens with different tougheners. It can be seen that tougheners with high $g_{c,\,TP}$ can enhance all the mechanical properties except stiffness, which is only related to E_{TP}. The use of a stiffer toughener favours high stiffness and strength, but reduces the strain at rupture and toughness. Compared with modulus and strength, strain at rupture and toughness are largely affected by the co-continuous patterns, as indicated by the size of the error bars. This aligns well with the above discussion, where the TP networks play the role of impediment after point 2. Note that the outliers of IPC-TPB2 in Fig. 4c & d, indicated by the large error bars, were induced by the extremely large value in the IPC5-TPB2 specimens, where crack blocking occurred.

In Fig. 5, the volume fraction (V_f) of the broken area of IPC and EP specimens is summarized. For comparison, the EP specimen was assumed to be composed of half EP networks and half TP networks (TPD1). Elements with d > 0.9 were considered as broken, and the V_f of the broken area was calculated by:

$$V_f\,\text{of total/EP/TP broken area} = \frac{\text{the number of total/EP/TP broken elements}}{\text{the number of total elements}} \tag{2}$$

where the number of total elements in the present work was 10,000.

Fig. 5a displays the V_f of the total broken area in different IPCs, and the effect of tougheners seems irregular. When the broken area in EP and

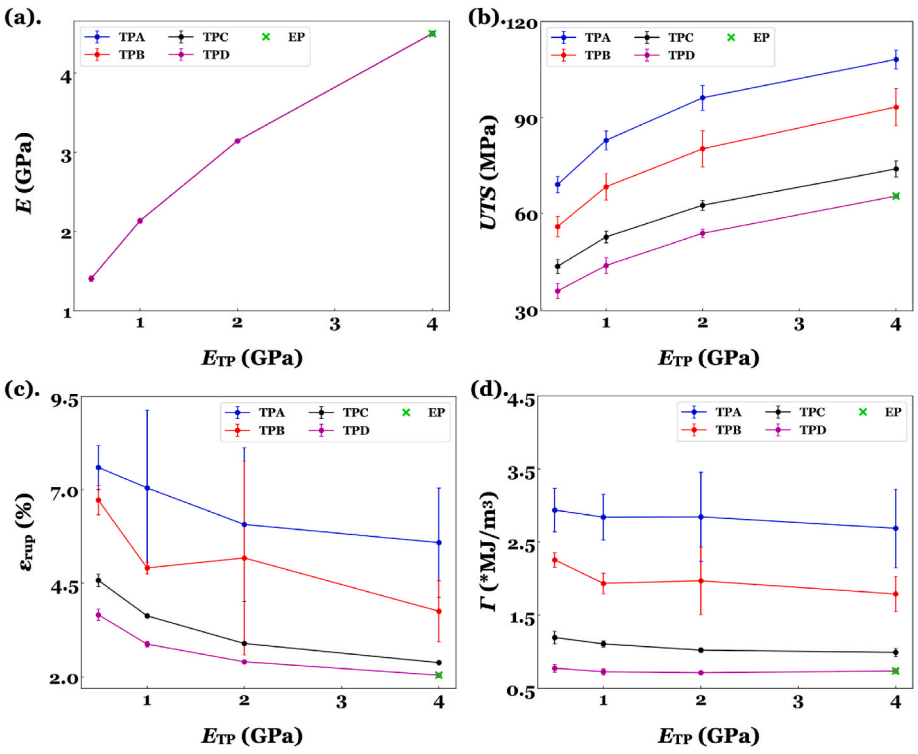

Fig. 4. Mechanical properties of IPC specimens. (a) Modulus; (b) Ultimate tensile strength; (c) Strain at rupture; (d) Toughness.

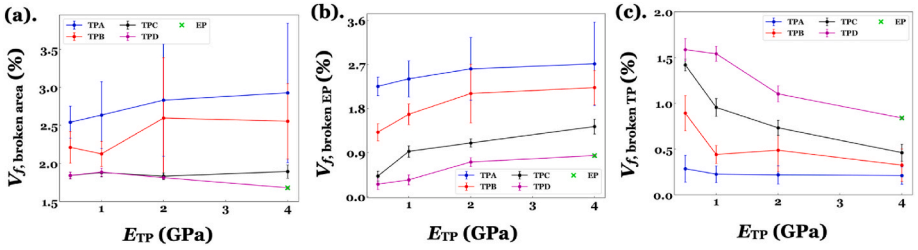

Fig. 5. The volume fraction of (a) Total broken area; (b) Broken EP area; (c) Broken TP area.

TP networks is investigated separately, it can be seen that stiffer tougheners lead to more fracture in the epoxy-rich phase (Fig. 5b), but less fracture in the toughening phase (Fig. 5c). The effect of increasing modulus of the tougheners on the overall mechanical performance is a result of competition between increasing breakage in the epoxy-rich phase and declining breakage in the toughening phase. This competing effect explains the irregularity of V_f of the total broken area and the relatively inconspicuous relationship between toughness and E_{TP}.

3.3. Sacrificial toughening mechanism

As mentioned in the introduction, a brittle matrix can break abundantly and act as a sacrificial phase to consume energy in co-continuous structures. In the present work, load transferring and impediment of TP networks are identified as the reasons for sacrificial fracture mechanisms, and as a result, the *UTS* can be enhanced, and crack patterns are displayed.

3.3.1. From the viewpoint of stress-strain behaviour

Based on the discussion in Section 3.1, the stress-strain curve can be divided into three stages (Fig. 6a): In stage 1, the load transferring through tough TP networks plays an important role in relieving the stress around crack tip and postponing the crack nucleation. In stage 2, even when the crack is starting to propagate, the stress concentration can be weakened, and the stress kept increasing until unstable crack growth in EP networks occurred. This enhanced stress effect after crack nucleation is an important toughening mechanism in co-continuous structures and helps to achieve strength-toughness balance. In stage 3, TP networks may not effectively release the stress anymore, but still can impede the crack growth and so dissipate energy. The strain energy is accordingly divided into three terms, e_1, e_2, and e_3, and their dependence on tougheners is shown in Fig. 6b-e. All the energy terms are favoured by tougher TP networks, and to be noted, e_2 is almost 0 when $g_{c,\,TP} = g_{c,\,EP}$, indicating tough TP networks are of great significance to the stress-enhancing effect. With increasing E_{TP}, the energy before crack nucleation (e_1) tends to be constant, but the energy during stress enhancing (e_2) declines (Fig. 6b & c). The non-monotonic trend of e_2 in the TPB series resulted from the outlier values in IPC4-TPB4 specimen, where e_1 was abnormally large and e_2 was almost zero because crack nucleation was blocked. In Fig. 6e, a negative relationship can be observed between (e_1+e_2) and E_{TP}, and the error bars of (e_1+e_2) are much smaller, indicating the effect of the load transferring mechanism can be enhanced by tougher and softer tougheners, and is barely related to the co-continuous patterns. The irregular trends with E_{TP} and large error bars of e_3 in Fig. 6d demonstrate the importance of co-continuous patterns in this stage, which is reasonable considering that tougheners work as impediments to crack growth.

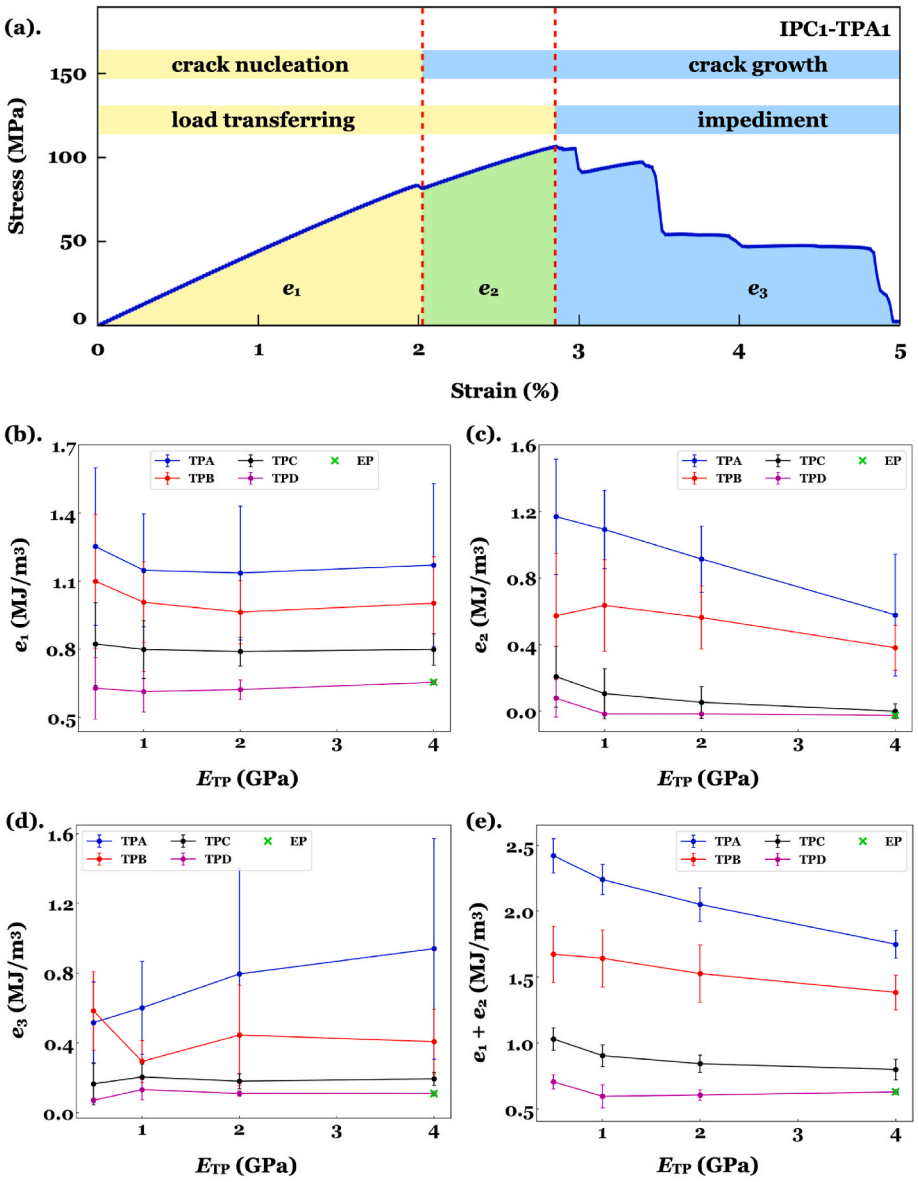

Fig. 6. Energy decomposition of IPC specimens. (a) Schematic of how total energy is divided into e_1, e_2 and e_3; the effect of toughener properties on (b) e_1; (c) e_2; (d) e_3; (e) $e_1 + e_2$.

3.3.2. *From the viewpoint of the crack topology*

Five toughening mechanisms based on crack propagation topology were identified, as shown in Fig. 7, namely (a) crack deflection, (b) crack bridging, (c) crack branching, (d) microcracking, and (e) crack blocking. Crack blocking refers to a situation where an existing crack is trapped by tougheners and a new catastrophic crack forms somewhere else.

The effect of TP properties on the crack growth patterns is summarized in Fig. 7f. Five specimens with the same tougheners were studied as a group, and the frequency of crack deflection, crack bridging, crack branching, microcracking, and crack blocking among each group was counted. Frequency varied from 0 to 5, while 0 stands for the toughening mechanism not being observed in the group, and 5 stands for the toughening mechanism being observed in all five specimens in the group. Crack deflection always can be observed, as long as mismatches between EP and TP exist. All toughening mechanisms were favoured by tougher TP networks, especially crack branching, and crack blocking, which were not observed in specimens with $g_{c,\,TP} = 80$ J/m^2 and $g_{c,\,TP} = 40$ J/m^2. With stiffer tougheners, the frequency of crack bridging and microcracking declined, while the frequency of crack branching increased. This may suggest that crack bridging and microcracking benefit from ductile tougheners, and crack branching requires high toughener strength.

3.4. *Fracture performance in different microstructures*

Fractures in co-continuous, particulate, and laminar microstructures were compared to identify the effect of microstructures. For all specimens, E_{TP} was fixed at 0.5 GPa, and $g_{c,\,TP}$ varied from 40 J/m^2 to 500 J/m^2. The toughness of all specimens benefited from increasing $g_{c,\,TP}$, but the most effective toughening microstructure changes with $g_{c,\,TP}$ (Fig. 8a). When $g_{c,\,TP}$ is smaller than 100 J/m^2, the toughness among the IPC, PRC and LCV specimens is similar. Upon increasing $g_{c,\,TP}$, the toughness of all specimens with different microstructures increases, but the IPC and PRC specimens present a marginal decreasing effect of toughness $g_{c,\,TP}$, while LCV specimens do not. The highest toughness occurred in IPC specimens at $g_{c,TP} = 200$ J/m^2, and in the LCV specimen at $g_{c,TP} = 500$ J/m^2. The mechanisms responsible for these effects are explained below.

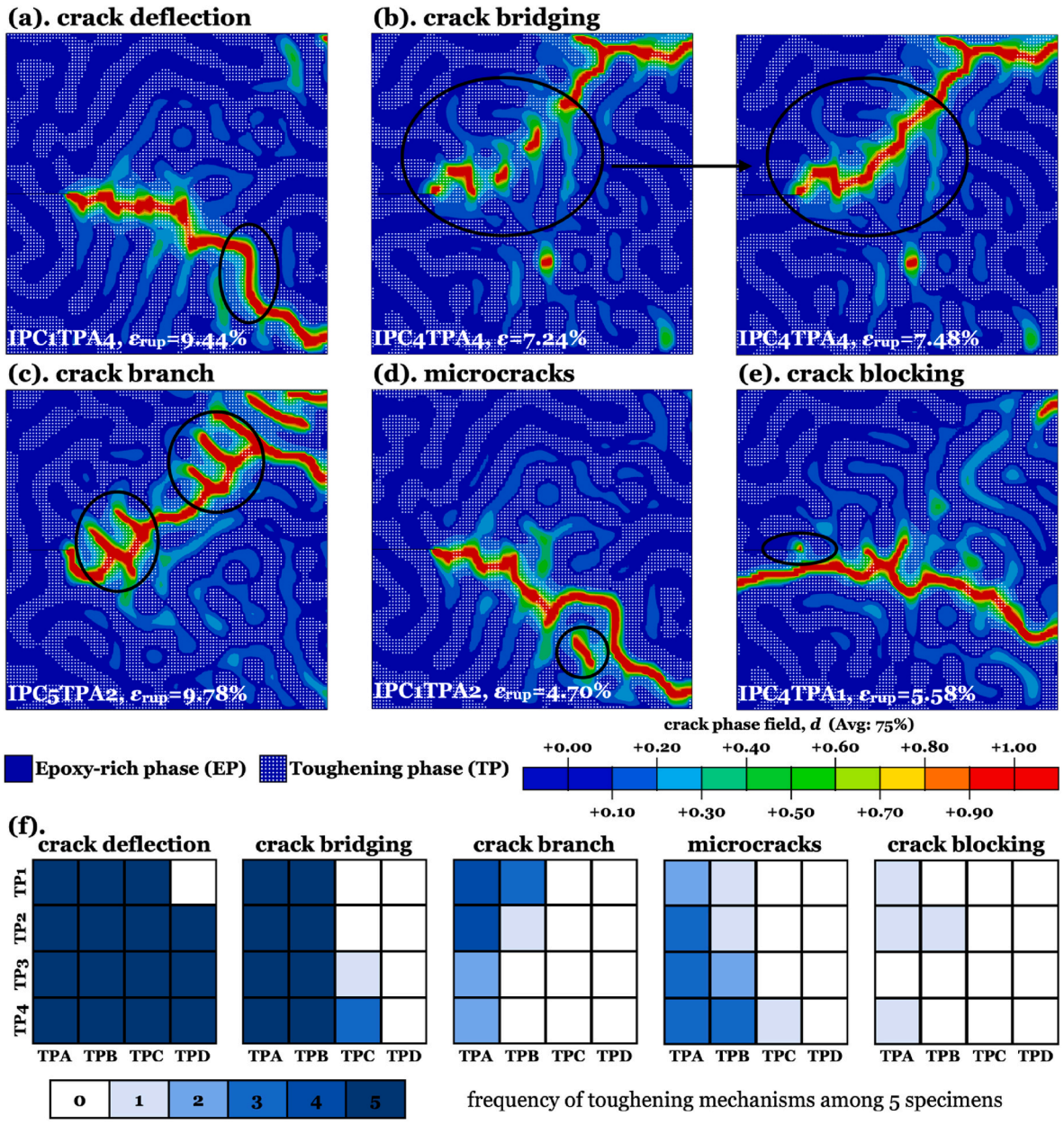

Fig. 7. Crack growth patterns in IPCs. (a) Crack deflection; (b) Crack bridging; (c) Crack branching; (d) Microcracking; (e) Crack blocking; (f) Dependence of crack growth patterns on toughener properties.

3.4.1. Comparison between IPC and PRC specimens

Although IPC and PRC specimens present similar toughness at $g_{c,TP} = 40$ J/m^2 and $g_{c,TP} = 80$ J/m^2, their divided energy terms are different. The IPCs show a larger ($e_1 + e_2$), as shown in Fig. 8b, benefiting from the load-transferring effect of the continuous tougheners, and PRCs show larger e_3 (Fig. 8f), benefiting from crack deflection induced by the soft toughener particles (Fig. S5). Note that this modelling assumes perfect adhesion between the two phases. When $g_{c,\ TP}$ increases to 200 J/m^2 and 500 J/m^2, the toughness of the IPCs increases mainly resulting from ($e_1 + e_2$), indicating an enhanced load transferring effect. Compared with co-continuous specimens, particle-reinforced specimens present a much smaller increment of toughness, as neither ($e_1 + e_2$) nor e_3 shows a significant increase. The reasons are, in PRCs, although the toughening particles are becoming tougher, their discrete nature means that it is hard to transfer load effectively, and pull-out can substitute for rupture of the toughening particles to facilitate crack growth (Fig. 8i & Fig. S5). Note also that other mechanisms such as cavitation, not modelled here, may also occur for PRCs [36,37].

3.4.2. Comparison between IPC and LC specimens

At a high toughness of $g_{c,\ TP} = 500$J/m^2, the energy consumed during stage 3 of LCV specimen is the main reason why it is the most effective toughening morphology, where the rupture of tougheners plays an important role. As shown in Fig. 8i, the volume fraction of broken TP declines with increasing $g_{c,\ TP}$ in IPCs and PRCs because tougher materials are more difficult to break. However, the $V_{f,\ broken\ TP}$ in LCV specimens was independent of $g_{c,\ TP}$, because the unique microstructure forces the crack to penetrate tougheners rather than detour tougheners (Fig. S5), and this makes LCV benefit most from increasing $g_{c,\ TP}$. Note that although the maximum toughening effect was obtained in the vertical laminar microstructure (LCV), the poorest toughening effect was observed in the horizontal laminar microstructure (LCH), whose mechanical properties barely benefit from tougheners. The high anisotropy in the laminar microstructure suggests that the use of any

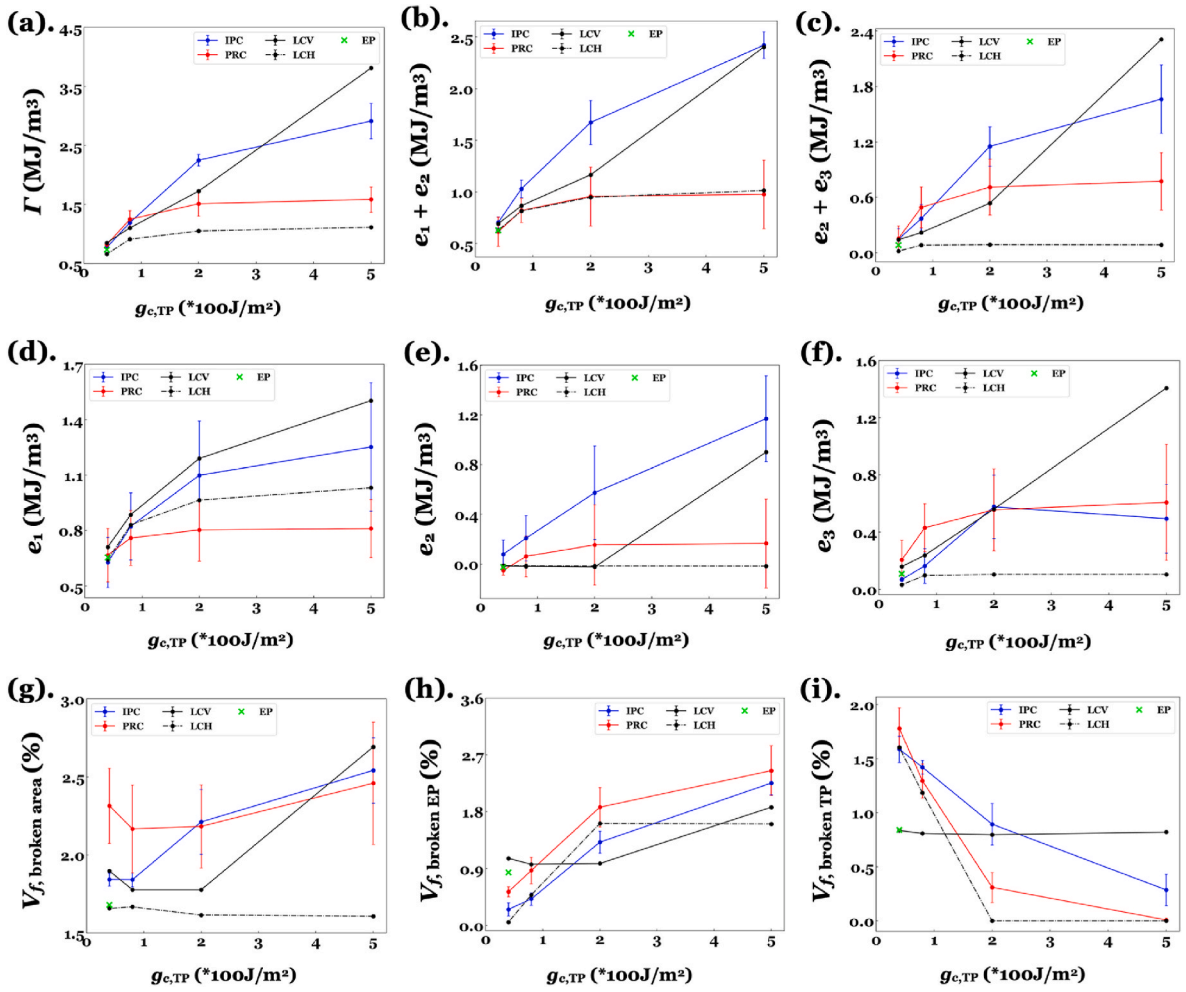

Fig. 8. Comparison of fracture properties between IPC, PRC, LCV, and LCH specimens. (a) Toughness; (b) $e_1 + e_2$; (c) $e_2 + e_3$; (d) e_1; (e) e_2; (f) e_3; (g) V_f of total broken area; (h) V_f of broken EP area; (i) V_f of broken TP area.

laminar microstructure must be carefully considered during application. This concurs with work which has studied the delamination of composites, where the orientation of the laminar structure parallel or perpendicular to the crack has a very large effect on the toughness.

4. Conclusion

A numerical model based on phase field method has been proposed to study crack growth in interpenetrating phase composites. It was found that with tougher toughenners, the composites always present enhanced strength and stretchability, while with stiffer toughenners, the composites present enhanced strength, but declined stretchability. It was also found that tougher and stiffer toughenners lead to more fracture in the brittle phase, but less fracture in the toughening phase, and overall fracture performance was a result of competition between them.

The sacrificial toughening mechanisms were identified from the view of stress-strain behaviour and crack topology. Before the maximum stress was reached, the toughening phase transferred the load from the crack tip to the whole specimen to achieve larger energy consumption, and afterwards the toughenners played the role of impediments to crack growth. Besides, five crack growth patterns were observed: crack deflection, crack bridging, crack branching, microcracking, and crack blocking. The frequency of the patterns changed with different toughenners.

Furthermore, the toughening effects in co-continuous (IPC), particulate (PRC), and laminar (LCV & LCH) microstructures were compared. With increasing toughness of toughenners, the fracture performance presented the most significant enhancement in LCV specimen, while negligible benefit in LCH specimen. How toughenners were involved in the fracture process is a crucial factor to the results. In addition, compared with PRC specimens, IPC specimens showed better performance because the co-continuous microstructure contributed to a better load-transferring effect.

Funding

This research did not receive any specific grant from funding agencies in the public, commercial, or not-for-profit sectors.

Declaration of competing interest

The authors declare that they have no known competing financial interests or personal relationships that could have appeared to influence the work reported in this paper.

Data availability

Data will be made available on request.

Acknowledgements

The authors would like to express great thanks to Dr. Zhenyang Xin

for his training and sharing of finite element analysis, Dr. Xudong Liang for his suggestions on conceptualization of this work, Dr. Lecheng Ruan for his suggestions on coding method, Dr. Gergely Molnár, Dr. Emilio Martínez Pañeda, and Dr. Jianguang Fang for their generous sharing of the crack phase field method.

Appendix A. Supplementary data

Supplementary data to this article can be found online at https://doi.org/10.1016/j.compscitech.2022.109873.

References

[1] O. Al-Ketan, A. Soliman, A.M. AlQubaisi, R.K. Abu Al-Rub, Nature-Inspired lightweight cellular Co-continuous composites with architected periodic gyroidal structures, Adv. Eng. Mater. 20 (2) (2018) 1–9, https://doi.org/10.1002/adem.201700549.

[2] J.H. Lee, L. Wang, M.C. Boyce, E.L. Thomas, Periodic bicontinuous composites for high specific energy absorption, Nano Lett. 12 (8) (2012) 4392–4396, https://doi.org/10.1021/nl302234f.

[3] W. Huang, M. Shishehbor, N. Guarín-Zapata, et al., A natural impact-resistant bicontinuous composite nanoparticle coating, Nat. Mater. 19 (11) (2020) 1236–1243, https://doi.org/10.1038/s41563-020-0768-7.

[4] M.J. Lee, J. Han, K. Lee, et al., Elastomeric electrolytes for high-energy solid-state lithium batteries, Nature 601 (7892) (2022) 217–222, https://doi.org/10.1038/s41586-021-04209-4.

[5] A. Gumyusenge, D.T. Tran, X. Luo, et al., Semiconducting polymer blends that exhibit stable charge transport at high temperatures, Science 362 (6419) (2018) 1131–1134, https://doi.org/10.1126/science.aau0759.

[6] D.W. Abueidda, P. Karimi, J.M. Jin, N.A. Sobh, I.M. Jasiuk, M. Ostoja-Starzewski, Shielding effectiveness and bandgaps of interpenetrating phase composites based on the Schwarz Primitive surface, J. Appl. Phys. 124 (17) (2018), https://doi.org/10.1063/1.5046105.

[7] I.V. Okulov, J. Weissmüller, J. Markmann, Dealloying-based interpenetrating-phase nanocomposites matching the elastic behavior of human bone, Sci. Rep. 7 (1) (2017) 1–7, https://doi.org/10.1038/s41598-017-00048-4.

[8] E. Su, C. Bilici, G. Bayazit, S. Ide, O. Okay, Solvent-free UV polymerization of n-octadecyl acrylate in butyl rubber: a simple way to produce tough and smart polymeric materials at ambient temperature, ACS Appl. Mater. Interfaces 13 (18) (2021) 21786–21799, https://doi.org/10.1021/acsami.1c03814.

[9] J. Huang, J. Fan, S. Yin, Y. Chen, Design of remotely, locally triggered shape-memory materials based on bicontinuous polylactide/epoxidized natural rubber thermoplastic vulcanizates via regulating the distribution of ferroferric oxide, Compos. Sci. Technol. 182 (July) (2019), https://doi.org/10.1016/j.compscitech.2019.107732.

[10] I. Hussain, O. Al-Ketan, F. Renda, et al., Design and prototyping soft–rigid tendon-driven modular grippers using interpenetrating phase composites materials, Int. J. Robot Res. 39 (14) (2020) 1635–1646, https://doi.org/10.1177/0278364920907697.

[11] S. Zhou, Z. Chen, R. Tusiime, et al., Highly improving the mechanical and thermal properties of epoxy resin via blending with polyetherketone cardo, Compos. Commun. (2019) 80–84, https://doi.org/10.1016/j.coco.2019.03.003, 13(March).

[12] M. Jiang, Y. Liu, C. Cheng, et al., Enhanced mechanical and thermal properties of monocomponent high performance epoxy resin by blending with hydroxyl terminated polyethersulfone, Polym. Test. (2018;69(March) 302–309, https://doi.org/10.1016/j.polymertesting.2018.05.039.

[13] W. Wang, J. Huang, Z. Gong, J. Fan, L. Cao, Y. Chen, Biobased PLA/NR-PMMA TPV with balanced stiffness-toughness: in-situ interfacial compatibilization, performance and toughening model, Polym. Test. 81 (September 2019) (2020), 106268, https://doi.org/10.1016/j.polymertesting.2019.106268.

[14] J. Chen, A.C. Taylor, Epoxy modified with triblock copolymers: morphology, mechanical properties and fracture mechanisms, J. Mater. Sci. 47 (11) (2012) 4546–4560, https://doi.org/10.1007/s10853-012-6313-6.

[15] Y. Liu, L. Cao, D. Yuan, Y. Chen, Design of super-tough co-continuous PLA/NR/SiO2 TPVs with balanced stiffness-toughness based on reinforced rubber and interfacial compatibilization, Compos. Sci. Technol. 165 (April) (2018) 231–239, https://doi.org/10.1016/j.compscitech.2018.07.005.

[16] D. Yuan, C. Xu, Z. Chen, Y. Chen, Crosslinked bicontinuous biobased polylactide/natural rubber materials: super toughness, "net-like"-structure of NR phase and excellent interfacial adhesion, Polym. Test. 38 (2014) 73–80, https://doi.org/10.1016/j.polymertesting.2014.07.004.

[17] A.M. Zolali, V. Heshmati, B.D. Favis, Ultratough co-continuous PLA/PA11 by interfacially percolated poly(ether-b-amide), Macromolecules 50 (1) (2017) 264–274, https://doi.org/10.1021/acs.macromol.6b02310.

[18] X. Li, K. Cui, T.L. Sun, et al., Mesoscale bicontinuous networks in self-healing hydrogels delay fatigue fracture, Proc. Natl. Acad. Sci. U. S. A. 117 (14) (2020) 7606–7612, https://doi.org/10.1073/pnas.2000189117.

[19] A. Agarwal, I.V. Singh, B.K. Mishra, Numerical prediction of elasto-plastic behaviour of interpenetrating phase composites by EFGM, Compos. B Eng. 51 (2013) 327–336, https://doi.org/10.1016/j.compositesb.2013.03.022.

[20] F. Xie, Z. Lu, Z. Yuan, Numerical analysis of elastic and elastoplastic behavior of interpenetrating phase composites, Comput. Mater. Sci. 97 (2015) 94–101, https://doi.org/10.1016/j.commatsci.2014.10.021.

[21] Y. Zhang, M.T. Hsieh, L. Valdevit, Mechanical performance of 3D printed interpenetrating phase composites with spinodal topologies, Compos. Struct. 263 (August 2020) (2021), https://doi.org/10.1016/j.compstruct.2021.113693.

[22] Y. Lu, J. Yang, W. Lu, R. Liu, G. Qiao, C. Bao, The mechanical properties of co-continuous Si_3N_4/Al composites manufactured by squeeze casting, Mater. Sci. Eng., A 527 (23) (2010) 6289–6299, https://doi.org/10.1016/j.msea.2010.06.047.

[23] Y. Wang, K. Chen, C. Xu, Y. Chen, Supertoughened biobased poly(lactic acid)-epoxidized natural rubber thermoplastic vulcanizates: fabrication, Co-continuous phase structure, interfacial in situ compatibilization, and toughening mechanism, J. Phys. Chem. B 119 (36) (2015) 12138–12146, https://doi.org/10.1021/acs.jpcb.5b06244.

[24] T. Li, Y. Chen, L. Wang, Enhanced fracture toughness in architected interpenetrating phase composites by 3D printing, Compos. Sci. Technol. 167 (June) (2018) 251–259, https://doi.org/10.1016/j.compscitech.2018.08.009.

[25] R. Tominaga, Y. Nishimura, Y. Suzuki, Y. Takeda, M. Kotera, A. Matsumoto, Co-continuous network polymers using epoxy monolith for the design of tough materials, Sci. Rep. 11 (1) (2021) 1–10, https://doi.org/10.1038/s41598-021-80978-2.

[26] D.R. King, T. Okumura, R. Takahashi, T. Kurokawa, J.P. Gong, Macroscale double networks: design criteria for optimizing strength and toughness, ACS Appl. Mater. Interfaces 11 (38) (2019) 35343–35353, https://doi.org/10.1021/acsami.9b12935.

[27] T. Okumura, R. Takahashi, K. Hagita, D.R. King, J.P. Gong, Improving the strength and toughness of macroscale double networks by exploiting Poisson's ratio mismatch, Sci. Rep. 11 (1) (2021) 1–13, https://doi.org/10.1038/s41598-021-92773-0.

[28] J.P. Gong, Why are double network hydrogels so tough? Soft Matter 6 (12) (2010) 2583–2590, https://doi.org/10.1039/b924290b.

[29] E. Ducrot, Y. Chen, M. Bulters, R.P. Sijbesma, C. Creton, Toughening elastomers with sacrificial bonds and watching them break, Science 344 (6180) (2014) 186–189, https://doi.org/10.1126/science.1248494.

[30] X. Zhou, B. Guo, L. Zhang, G.H. Hu, Progress in bio-inspired sacrificial bonds in artificial polymeric materials, Chem. Soc. Rev. 46 (20) (2017) 6301–6329, https://doi.org/10.1039/c7cs00276a.

[31] K. Ou, X. Dong, C. Qin, X. Ji, J. He, Properties and toughening mechanisms of PVA/PAM double-network hydrogels prepared by freeze-thawing and anneal-swelling, Mater. Sci. Eng. C 77 (2017) 1017–1026, https://doi.org/10.1016/j.msec.2017.03.287.

[32] J.W. Cahn, J.E. Hilliard, Free energy of a nonuniform system. II. Thermodynamic basis, J. Chem. Phys. 30 (5) (1959) 1121–1124, https://doi.org/10.1063/1.1730145.

[33] A. Logg, G.N. Wells, DOLFIN: automated finite element computing, ACM Trans. Math Software 37 (2) (2010), https://doi.org/10.1145/1731022.1731030.

[34] H.P Langtangen, A FEniCS tutorial, in: A. Logg, KA. Mardal, G. Wells (Eds.), Automated Solution of Differential Equations by the Finite Element Method, Lecture Notes in Computational Science and Engineering, 84, Springer, Berlin, Heidelberg, 2012, https://doi.org/10.1007/978-3-642-23099-8_1.

[35] G. Molnár, A. Gravouil, R. Seghir, J. Réthoré, An open-source Abaqus implementation of the phase-field method to study the effect of plasticity on the instantaneous fracture toughness in dynamic crack propagation, Comput. Methods Appl. Mech. Eng. 365 (2020), https://doi.org/10.1016/j.cma.2020.113004.

[36] W.L. Tsang, A.C. Taylor, Fracture and toughening mechanisms of silica- and core–shell rubber-toughened epoxy at ambient and low temperature, J. Mater. Sci. 54 (2019) 13938–13958, https://doi.org/10.1007/s10853-019-03893-y.

[37] A.J. Kinloch, A.C. Taylor, The toughening of cyanate-ester polymers, Part II: Chemical modification, J. Mater. Sci. 38 (2003) 65–79, https://doi.org/10.1023/A:1021109731672.